Effect of Soil Moisture on Diurnal Convection and Precipitation in Large-Eddy Simulations

GUIDO CIONI

Max Planck Institute for Meteorology, and International Max Planck Research School on Earth System Modelling, Hamburg, Germany

CATHY HOHENEGGER

Max Planck Institute for Meteorology, Hamburg, Germany

(Manuscript received 11 October 2016, in final form 15 February 2017)

ABSTRACT

A determination of the sign and magnitude of the soil moisture–precipitation feedback relies either on observations, where synoptic variability is difficult to isolate, or on model simulations, which suffer from biases mainly related to poorly resolved convection. In this study, a large-eddy simulation model with a resolution of 250 m is coupled to a land surface model and several idealized experiments mimicking the full diurnal cycle of convection are performed, starting from different spatially homogeneous soil moisture conditions. The goal is to determine under which conditions drier soils may produce more precipitation than wetter ones. The methodology of previous conceptual studies that have quantified the likelihood of convection to be triggered over wet or dry soils is followed but includes the production of precipitation. Although convection can be triggered earlier over dry soils than over wet soils under certain atmospheric conditions, total precipitation is found to always decrease over dry soils. By splitting the total precipitation into its magnitude and duration component, it is found that the magnitude strongly correlates with surface latent heat flux, hence implying a wet soil advantage. Because of this strong scaling, changes in precipitation duration caused by differences in convection triggering are not able to overcompensate for the lack of evaporation over dry soils. These results are further validated using two additional atmospheric soundings and a series of perturbed experiments that consider cloud radiative effects, as well as the effect of large-scale forcing, winds, and plants on the soil moisture–precipitation coupling.

1. Introduction

The evolution of the atmosphere is partly written in the land surface. Over some regions of the globe and by changing the soil moisture, it is possible to modify the future atmospheric state on time scales ranging from the diurnal cycle to the seasonal scale. For instance, Fischer et al. (2007) used model simulations of the anomalously hot summer of 2003 to show that, by simply decreasing soil moisture by 25% in spring, summer temperature anomalies can increase by more than 2°C. In this particular case, reduced soil moisture availability limits the surface latent heat flux which, as a compensation, leads to a larger surface sensible heat flux and hence warmer air temperatures. Although the coupling between air temperature and soil moisture is straightforward (Miralles et al. 2012, 2014), the coupling between precipitation and soil moisture has been debated many times. A wetter soil promotes larger surface latent heat fluxes in a soil moisture–limited regime (Budyko 1974), thus increasing the moisture contribution to the atmosphere. From an atmospheric moisture balance perspective, this increase in the amount of water vapor increases the potential amount of precipitation. The precipitation eventually falls on the ground and replenishes the soil moisture reservoir, closing the feedback loop. This is the main idea behind the mechanism of precipitation recycling (Trenberth 1999). It implies a positive soil moisture–precipitation feedback. Precipitation recycling is nevertheless thought not to play a big role on the regional scale. Van der Ent et al. (2010), for instance, reported a recycling ratio of less than 10% for horizontal scales of 500 km, which agrees with the

Corresponding author: Guido Cioni, guido.cioni@mpimet.mpg.de

DOI: 10.1175/JHM-D-16-0241.1

estimate obtained by Schär et al. (1999) based on a one-month model simulation over Europe. The major source of water vapor for precipitation is indeed constituted by the advection of moisture into a region rather than direct local evapotranspiration.

Instead of locally increasing water vapor, soil moisture can modify the efficiency at which water vapor is converted into precipitation. By exploring this scenario with the aid of a simple 1D model, Findell and Eltahir (2003a) showed that, over a homogeneous surface, the resulting coupling over a diurnal cycle strongly depends on the early morning atmospheric state. Larger values of sensible heat flux, as the ones found over dry soils, produce a deeper planetary boundary layer (PBL) that can more easily reach the level of free convection (LFC). On the other hand, larger values of latent heat flux, as the ones found over wet soils, lead to a moistening of the PBL and thus to a lowering of the lifting condensation level (LCL), making it easier to trigger convection. Different combinations of low-level instability and moisture amount favor one or the other mechanism, resulting either in a dry soil advantage (more precipitation over dry soils) or in a wet soil advantage (more precipitation over wet soils). In Findell and Eltahir (2003a) these two scenarios are differentiated using the convective triggering potential (CTP) index, which considers convective instability between 900 and 700 hPa, and the HI_{low} humidity index, which corresponds to the sum of the dewpoint depressions at 950 and 850 hPa. A third mechanism by which soil moisture can impact precipitation is through the generation of thermally induced mesoscale circulations (Pielke 2001; Taylor et al. 2011), which is not considered in this study as the focus is on initially homogeneous surface conditions and short time scales.

Given the importance of the soil moisture–precipitation feedback in regulating the global and continental hydrological cycle, many studies have tried to estimate its more likely sign and magnitude using either observations (e.g., Miralles et al. 2014; Ford et al. 2015), coarse-resolution models with parameterized convection (e.g., Schär et al. 1999; Wang et al. 2007), convection-permitting models with explicit convection (e.g., Hohenegger et al. 2009; Schlemmer et al. 2012), or conceptual models (e.g., Findell and Eltahir 2003a; Tawfik et al. 2015; Gentine et al. 2013). The main problem regarding observational studies is that the effect of synoptic variability is difficult to filter out. In contrast, model studies rely on their parameterizations. Hohenegger et al. (2009), using model simulations of an entire summer season over the Alps, showed that the sign of the soil moisture–precipitation feedback strongly depends on the design of the model. In particular, the parameterization of convection is the model feature that greatly affects the sign of the feedback. The parameterization of convection can even reverse its sign depending on the use or not as well as on the design of such a parameterization. Even convection-permitting simulations are not exempt of biases because of a grid spacing that is still too coarse to properly resolve convection. This typically leads to a too late triggering of convection (e.g., Hohenegger et al. 2008), which might bias the resulting soil moisture–precipitation feedback. Finally, it should be noted that studies often use metrics to diagnose the soil moisture–precipitation feedback that were designed to assess the potential for triggering of convection over a certain surface state, without actually considering the amount of precipitation. Some examples of such metrics are the already described CTP–HI_{low} framework of Findell and Eltahir (2003a) and the heated-condensation framework of Tawfik et al. (2015), where the buoyant condensation level and buoyant mixing temperature are used to quantify the preconditioning of the atmospheric state to moist convection.

The present work aims at estimating the sign and magnitude of the soil moisture–precipitation coupling in an idealized setup of an initially horizontally homogeneous atmosphere and homogeneous soil moisture conditions. The focus is on one diurnal cycle of convection with its associated precipitation. The first goal is to quantify the likelihood of precipitation on soils that are either wetter or drier than normal. Here we neglect any effects that would arise due to the presence of heterogeneous soil moisture conditions, which, in the absence of winds, lead to more precipitation over spatially drier soil patches (Taylor et al. 2012). The second goal is to evaluate whether large-scale effects, cloud–surface interactions, or the presence of winds or plants can modify the sign and magnitude of the coupling.

To address these goals, idealized experiments are performed with the aid of a state-of-the-art, high-resolution large-eddy simulation (LES) model starting from different initial soil moisture values. The LES model is fully coupled to a land surface model as well as to radiation. This setup allows for an explicit representation of convection and of land surface interactions on scales of $O(100)$ m. Within this setup, the methodology proposed by Findell and Eltahir (2003a) is revisited. Instead of focusing only on the dependence of the triggering of convection on soil moisture, attention is set on the entire diurnal cycle of convection and its precipitation.

The paper is organized as follows. Section 2 describes the modeling framework and the experiment setup. In section 3 the results of the experiments using the same initial atmospheric conditions as in Findell and Eltahir (2003a) are discussed and a simple expression is derived to assess the likelihood of observing more precipitation over drier soils. In section 4 the role of clouds, large-scale forcing, winds, and plants on the

soil moisture–precipitation coupling is investigated. Conclusions are given in section 5.

2. Method

a. The modeling framework

The Icosahedral Nonhydrostatic (ICON) model is a new-generation unified modeling system for numerical weather prediction (NWP) and climate studies that allows for an explicit representation of nonhydrostatic processes and can be applied across a wide range of scales. It has been developed as a collaboration between the Max Planck Institute for Meteorology and the German Weather Service [Deutscher Wetterdienst (DWD)], where it is currently used to produce global operational forecasts. To maximize the model performance and to remove the singularity at the poles, ICON employs an unstructured icosahedral grid where all the common mathematical operators are expressed in terms of components either normal or perpendicular to the triangle edges (Wan et al. 2013).

The nonhydrostatic dynamical core has been validated by means of several idealized cases including a flow over orography and a baroclinic development, as well as through NWP skill scores [see Zängl et al. (2015) for details]. In the context of the High Definition Clouds and Precipitation for Advancing Climate Prediction [HD(CP)^2] project, a large-eddy version of the ICON model (ICON-LEM) has been developed. ICON-LEM uses the same dynamical core as ICON and shares many of its parameterizations, except for the representation of turbulence, cloud cover, convection, and gravity waves. A comprehensive description of the model can be found in Dipankar et al. (2015). Below, we only recall some of its aspects that are more relevant for our study.

ICON-LEM solves the Favre-filtered (Hinze 1975) equations of motion for the prognostic variables: horizontal velocity component normal to the triangle edges v_n, horizontal velocity component tangential to the triangle edges v_t, vertical wind component perpendicular to the triangle edges w, density ρ, virtual potential temperature θ_v, and the specific masses of tracers. In the momentum equations, the turbulence parameterization terms are computed as the divergence of the subgrid-scale stress tensor following the approach of Lilly (1962), who revisited the classical Smagorinsky scheme. The contributions of subgrid slow physics (e.g., radiation) and fast physics (e.g., cloud microphysics) are expressed through a flux–gradient relationship in the thermodynamic and tracer equations. The governing equations are integrated in time using a two-time-level predictor–corrector scheme, except for the terms corresponding to the vertical sound-wave propagation, which are integrated implicitly. The tracers are integrated using a flux-form semi-Lagrangian scheme for its better conservation properties.

At the typical resolution of $O(100)$ m adopted in ICON-LEM, deep convection is thought to be explicitly resolved (Bryan et al. 2003; Petch et al. 2002), while cloud fraction is diagnosed through a simple all-or-nothing scheme (Sommeria and Deardorff 1977). The microphysical cloud processes are parameterized using a one-moment scheme that distinguishes between cloud water, rain, cloud ice, graupel, hail, and snow [see Doms et al. (2011) for a comprehensive description]. The choice of this particular scheme is due to the fact that it has been extensively validated and used for many years in the operational setup of the Consortium for Small-Scale Modeling (COSMO)-DE model, which provides short-range forecasts over Germany at a resolution of 2.8 km. Furthermore, the aforementioned microphysical scheme produced the best agreement with other LES studies that investigated typical features of the convective diurnal cycle over midlatitude regions (e.g., Schlemmer et al. 2012). Subgrid-scale orographic effects and nonorographic gravity wave drag parameterizations are disabled in ICON-LEM. Radiation is parameterized with the aid of the Rapid Radiative Transfer Model (RRTM) scheme [see Clough et al. (2005) for a general review].

The coupling between soil and atmosphere is realized through surface fluxes of moisture, heat, and momentum. They are parameterized using a simple drag-law formulation (Dipankar et al. 2015; Doms et al. 2011). The surface latent heat flux entails contribution from bare soil evaporation, plant transpiration, and evaporation from the interception layer. These contributions are computed by the land surface model TERRA-Multi-Layer (TERRA-ML; Schrodin and Heise 2002). TERRA-ML also predicts the evolution of soil moisture and soil temperature at various soil layers. The water reservoir of every soil layer can be modified by gravitational and capillary flux, water extraction by plants, and runoff, while the balance of the first soil layer also accounts for bare soil evaporation, percolation, and precipitation. An interception layer at the surface is coupled to the underlying soil layers. The bare soil evaporation scheme employs the Biosphere–Atmosphere Transfer Scheme (BATS) formulation (Dickinson 1984). Surface evaporation can thus vary between the value of potential evaporation, which depends on surface temperature, and a limiting factor that corresponds to the maximum moisture flux through the surface that the soil can sustain. While more details about the formulation can be found in Doms et al. (2011), the drawbacks of using this particular scheme will be presented in section 3a. The

vertical soil water transport between different layers is parameterized using the Richards equation (Richards 1931). At the lower boundary, defined as the lowermost two soil layers, only downward gravitational transport is considered. Runoff from any soil layer occurs if the total water content of the layer exceeds the field capacity and if the divergence of the fluxes associated with soil water transport are negative. The temperature of the soil layers is predicted using a simple heat diffusion equation (Doms et al. 2011). The lower boundary condition for temperature is provided by a climatological temperature, constant in time, while at the upper boundary the forcing due to surface net radiation (sum of surface longwave and shortwave radiative fluxes), sensible heat flux, latent heat flux, and ground heat flux determines the temperature evolution.

The ICON-LEM modeling framework has been validated for the idealized cases of a dry convective boundary layer and of a cloud-topped boundary layer in Dipankar et al. (2015). The simulations revealed similar results to the ones obtained with two other large-eddy models (LEMs), the University of California, Los Angeles, Large-Eddy Simulation (UCLA-LES) model and the Parallelized Large-Eddy Simulation Model (PALM; Maronga et al. 2015). Furthermore, in the context of the HD(CP)^2 project, the modeling framework employing both ICON-LEM and TERRA-ML has been validated using a semi-idealized approach (Heinze et al. 2017a) and by performing real-case simulations (Heinze et al. 2017b). In the latter case, the ICON-LEM simulations compare well to simulations performed with the COSMO model, with ICON-LEM in particular producing more realistic mesoscale variability.

b. *Experimental design*

1) BASIC CONFIGURATION

To study the response of the diurnal cycle of convection and precipitation to soil moisture, different experiments have been set up using an idealized coupled configuration of ICON-LEM and TERRA-ML. The two early morning soundings (1200 UTC/0600 LST) proposed by Findell and Eltahir (2003a), taken on 3 July and 23 July 1999 in Lincoln, Illinois (United States), are used to initialize the atmosphere, as we want to repeat their analysis but including precipitation. The profiles are illustrated in Fig. 1. Since the effect of winds is not considered in the basic configuration, the (zonal u, meridional v, and vertical w) velocity components are set to 0 over the whole atmospheric column at the beginning of the simulation. The 3 July sounding should represent a wet soil advantage and thus favor convection over wetter soils, whereas the sounding taken on 23 July should favor convection over drier soils, as briefly explained in the introduction and in Findell and Eltahir (2003a). The two cases are referred to in the following as WA for wet soil advantage and DA for dry soil advantage. For each atmospheric profile, the simulations start at 0600 LST and end at 2400 LST. At the initial time, a random perturbation is added in the three lowermost atmospheric levels on the prognostic variables θ_v and w with an amplitude of 0.2 K and 0.05 m s^{-1}, respectively, to break the perfectly homogeneous initial state. To avoid that differences in the insolation between the two cases may affect the coupling, the radiation code is always initialized with the date of the WA sounding and coordinates of Lincoln, Illinois (40.15°N, 89.37°W). Thus, the solar zenith angle depends only on the time of the day and not on the position on the domain.

The horizontal domain comprises 400 × 400 points on a doubly periodic domain with a resolution of 250 m, which should explicitly resolve deep moist convection (Bryan et al. 2003; Petch et al. 2002), giving a total size of approximately 100 × 100 km^2. This should be large enough to allow organization of convection (Tompkins 2001). It should be recalled that, on an icosahedral grid, the resolution can be formulated with different metrics: throughout this work we will always refer to the distance between triangle edges. Rotation is not considered in the model since the Coriolis term f is set to 0. In the vertical, 150 levels are adopted: the spacing varies from 10 m in the lowermost layer to approximately 400 m at the model top situated by 21 km. In the uppermost 20 atmospheric levels, a sponge layer (Klemp et al. 2008) prevents upward-propagating gravity waves from being reflected.

As in the operational setup of ICON, the soil column is discretized into eight soil layers. In this configuration the soil layers have the following depths: 0.01, 0.02, 0.06, 0.18, 0.54, 1.62, 4.86, and 14.58 m. The soil temperature of the climatological layer amounts to 281 K, whereas the soil type is set to loam. This corresponds to the most common soil type used in ICON over midlatitude areas (e.g., Germany). Table 1 summarizes the parameters used by TERRA-ML in our configuration.

To obtain a spread of surface fluxes large enough to see a significant atmospheric response, soil moisture is varied starting from the saturation value and decreasing down to a condition of a dry soil but still over the wilting point. The soil moisture values considered are 100%, 80%, 70%, 60%, 50%, and 40% of the saturation value, respectively. For the sake of simplicity, they are set homogeneous over the whole soil column.

The soil temperature profile is prescribed by linearly interpolating the near-surface temperature from the lowermost atmospheric level to the climatological value

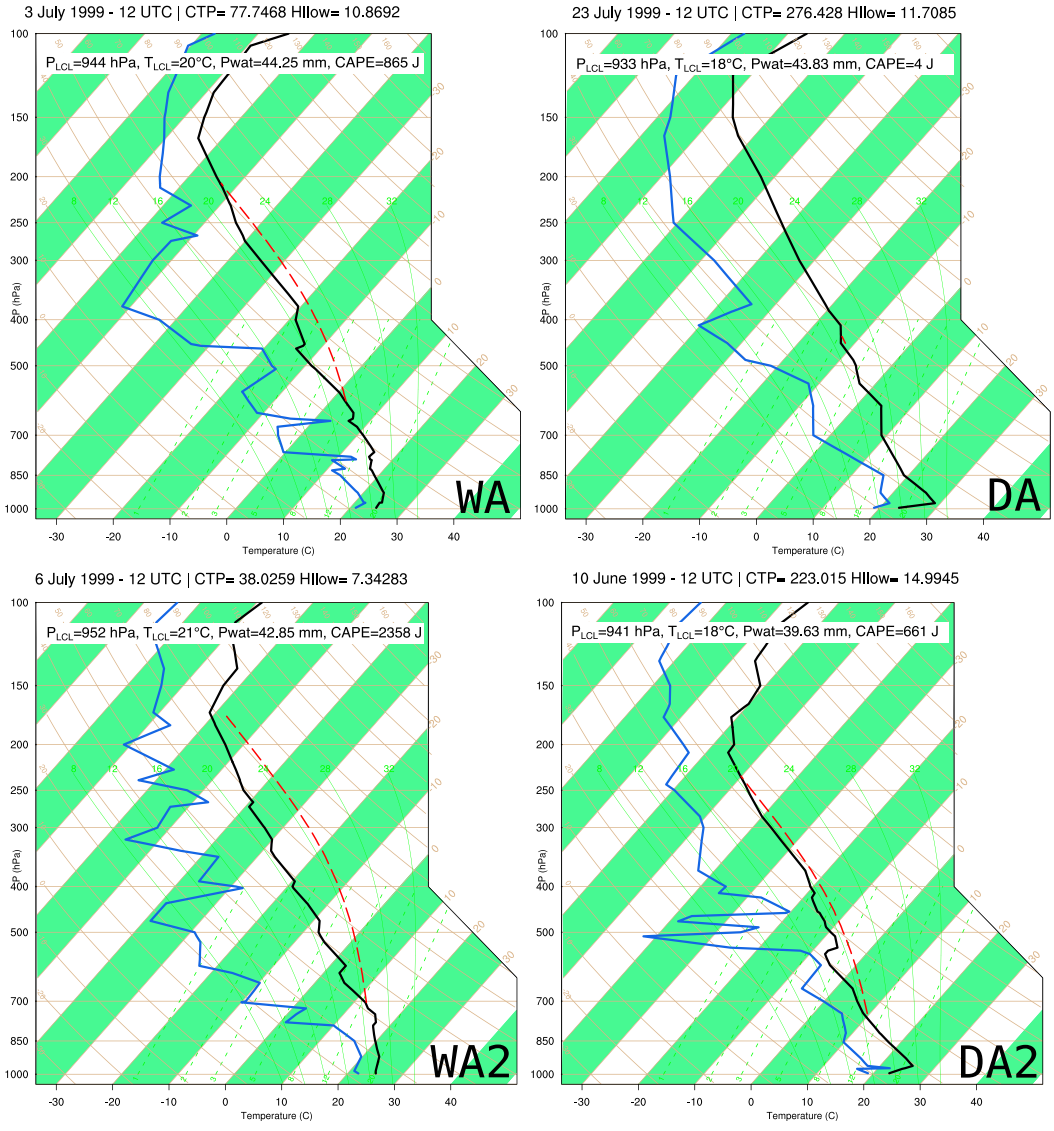

FIG. 1. Atmospheric profiles measured at Lincoln, Illinois. Temperature (°C) is represented by the black line and dewpoint temperature (°C) by the blue line. The red dashed line highlights the area where the surface parcel is positively buoyant with respect to the environment. The plot title contains the value of CTP and HI_{low} computed following Findell and Eltahir (2003a). Text insets indicate values of pressure and temperature at the LCL, vertically integrated water vapor content (Pwat), and CAPE.

of 281 K. Given the consideration of a single diurnal cycle, the values of soil moisture and temperature in deeper soil layers should not appreciably affect the surface latent heat fluxes. As a comparison, Findell and Eltahir (2003a) also used a vertically constant soil moisture, but their values were 100% and 20% with respect to saturation.

2) PERTURBED EXPERIMENTS

A series of additional experiments (see Table 2) are performed to test specific controls on the soil moisture–precipitation coupling. To save computing time and given the observed quasi-monotonic response of precipitation to soil moisture in DA and WA, only soil moisture values of 100%, 70%, and 40% of the saturation value are considered. For most of these experiments the DA sounding was used exclusively in order to see whether drier soils could produce more precipitation than wetter soils.

First, it should be noted that, given the HI_{low} threshold of 10°C proposed by Findell and Eltahir (2003a) to distinguish between the wet and dry soil advantage, the WA sounding, with a computed HI_{low} of 10.9°C, may not be viewed as the best sounding. For this reason, and in

TABLE 1. Parameters used in the land surface model TERRA-ML.

Soil type	Loam
Volume of voids/pore volume	$0.455\,m^3\,m^{-3}$
Field capacity	$0.340\,m^3\,m^{-3}$
Wilting point	$0.110\,m^3\,m^{-3}$
Air dryness point	$0.035\,m^3\,m^{-3}$
Heat capacity	$1.42 \times 10^6\,J\,m^{-3}\,K^{-1}$
Surface roughness length	0.1 m
Albedo	0.15
Longwave surface emissivity	1
Cases with plants	
Land-cover class	Mosaic of cropland (50%–70%) and vegetation (20%–50%)
Plant cover	100%
Leaf area index	3
Stomatal resistance	$160\,s\,m^{-1}$
Root depth	0.5 m
Surface roughness length	0.25 m

order to have a larger data sample, two additional early morning soundings are selected from the same period as used in Findell and Eltahir (2003a). The two retained dates are 6 July and 10 June 1999 and the respective profiles are shown in Fig. 1. For these atmospheric states the following values of CTP–HI_{low} are obtained: ($38\,J\,kg^{-1}$, 7°C) and ($223\,J\,kg^{-1}$, 15°C), respectively. Considering the thresholds proposed by Findell and Eltahir (2003a), these cases better fall into the different hypothesized regions of the coupling behavior, with 6 July falling into the wet soil advantage and 10 June in the dry soil advantage. The two simulations are called WA2 and DA2, respectively.

Second, the impact of clouds on the coupling is explored. By inspecting the surface radiative balance in model simulations, Schär et al. (1999) found that the reduction of incoming shortwave radiation due to cloud shading is overcompensated by an increase in longwave radiation. This consequently supports higher surface fluxes over wet soils in cloudier conditions than over dry soils in sunnier conditions. The latter response further emphasizes a positive soil moisture–precipitation feedback. However, from observations, a decrease of the net radiation by cloud radiative effect is generally expected. To quantify the potential amplification or dampening of the response of precipitation to an initial change in soil moisture by cloud radiative effects (CREs), simulations are performed starting from the DA sounding and using a modified version of ICON-LEM, where liquid and ice clouds are set transparent to the radiation both in the shortwave and longwave. These simulations are called DA_transp. Making cloud transparent to radiation has been successfully used in several studies (see, e.g., Stevens et al. 2012; Fermepin and Bony 2014) to isolate the impacts of CREs on the dynamic of convection.

Third, the impact of large-scale forcing is considered. The presence of subsidence favors the development of an inversion layer at the top of the boundary layer that could eventually suppress deep convection formation. In this regime, only a strong enough sensible heat flux that can break through the inversion may promote the development of deep convection, thus possibly leading to more precipitation over drier soils. The effect of large-scale forcing is mimicked by prescribing a large-scale velocity w_{LS} that acts on the tendency equations of momentum, temperature, and moisture (Randall and Cripe 1999). The subsidence velocity w_s^0 in the perturbed

TABLE 2. Experiment descriptions. In the text, the following notation is adopted to refer to a specific experiment: SOUNDING_CASE_MOISTURE, for example, WA_100 represents the simulation run with the wet soil advantage sounding (3 Jul 1999) and a fully saturated soil, while DA_wind_40 refers to the simulation run with the dry soil advantage sounding (23 Jul 1999) considering the presence of winds with a soil moisture of 40% of the saturation value.

Name	Date	No. of simulations	Soil moisture	Description
Basic configuration				
WA	3 Jul 1999	6	100%, 80%, 70%, 60%, 50%, and 40% saturation	Wet soil advantage
DA	23 Jul 1999	6	100%, 80%, 70%, 60%, 50%, and 40% saturation	Dry soil advantage
Perturbed experiments				
DA_transp	23 Jul 1999	3	100%, 70%, and 40% saturation	Transparent clouds
DA_subs	23 Jul 1999	3	100%, 70%, and 40% saturation	Induced subsidence
DA_asce	23 Jul 1999	3	100%, 70%, and 40% saturation	Induced ascent
DA_wind	23 Jul 1999	3	100%, 70%, and 40% saturation	Nonzero winds
DA_plants	23 Jul 1999	3	100%, 70%, and 40% saturation	With plants
WA_plants	3 Jul 1999	3	100%, 70%, and 40% saturation	With plants
WA2	6 Jul 1999	3	100%, 70%, and 40% saturation	Additional wet soil advantage
WA2_plants	6 Jul 1999	3	100%, 70%, and 40% saturation	With plants
DA2	10 Jun 1999	3	100%, 70%, and 40% saturation	Additional dry soil advantage
DA2_plants	10 Jun 1999	3	100%, 70%, and 40% saturation	With plants

experiments DA_subs is specified following the Rain in Cumulus over the Ocean (RICO) setup for different heights of the atmospheric column z (VanZanten et al. 2011):

$$w_{\mathrm{LS}} = \begin{cases} w_s^0 z & \text{for} \quad z < 1\,\mathrm{km} \\ w_s^0 & \text{for} \quad 1 < z < 3\,\mathrm{km} \\ w_s^0 (4 - z) & \text{for} \quad 3 < z < 4\,\mathrm{km} \\ 0 & \text{for} \quad z > 4\,\mathrm{km} \end{cases}, \qquad (1)$$

with $w_s^0 = -0.005\,\mathrm{m\,s^{-1}}$. This choice produces a constant subsidence velocity $w_{\mathrm{LS}} = w_s^0$ between 1 and 3 km that linearly decreases to 0 outside of this layer. Moreover, an additional set of simulations with a forced ascent, called DA_asce, is carried out where w_{LS} is simply set equal to a constant value of $0.005\,\mathrm{m\,s^{-1}}$ over the whole atmospheric column. Forced ascent can be thought as representing an additional buoyancy source for the parcel, associated, for example, to frontal induced lift. The reason behind not using a vertically constant subsidence velocity in DA_subs is because early test simulations showed that convection was strongly suppressed in such simulations, making a reliable estimation of the coupling practically impossible.

Fourth, the impact of winds on the soil moisture–precipitation coupling is investigated in a set of simulations called DA_wind. A follow-up study by Findell and Eltahir (2003b) on their original work already indicated that winds strongly influence the coupling. Strong low-level wind shear can suppress the convective potential, making it harder to rain regardless of the surface state, while veering winds with small low-level shears may provide more buoyancy and enhance convection. Moreover, wind shear can promote the organization of convection through interaction with cold pools (Rotunno et al. 1988; Schlemmer and Hohenegger 2014). Organized convection may be less dependent on surface fluxes as the convective evolution becomes dictated by the cold pools' evolution. In the case DA_wind, the simulations are initialized with the wind field measured by the balloon sounding. Note that winds are only prescribed in the initial condition and freely evolve during the day in every atmospheric level.

Finally, the dependency of the results on the specification of the land surface is investigated by fully covering the soil with plants in simulations WA_plants, DA_plants, WA2_plants, and DA2_plants. The land-cover class is set to a mosaic of cropland (50%–70%) and vegetation (20%–50%) with a maximum leaf area index of 3, minimum stomatal resistance of $160\,\mathrm{s\,m^{-1}}$, and a root depth of 0.5 m (these parameters are taken from the COSMO model). Surface roughness length is increased from 0.1 to 0.25 m. Within this setup, the only contribution to surface latent heat flux comes from the transpiration term, given that bare soil is fully covered by plant leaves. For the exact formulations of the different parameterizations adopted with plants (e.g., canopy resistance), the reader is referred to Doms et al. (2011).

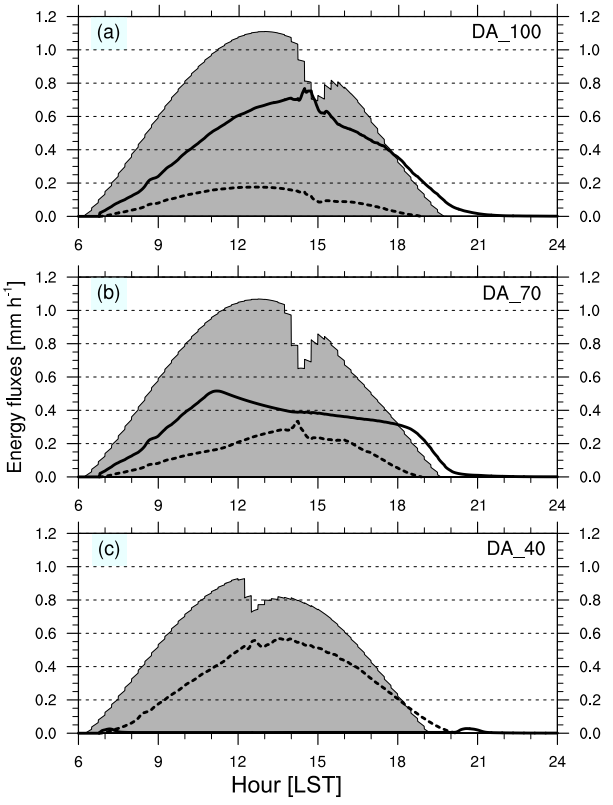

FIG. 2. Time series (LST) of domain-averaged surface latent heat flux (thick black line), sensible heat flux (thick black dashed line), and net radiation at the surface (gray shading) for the DA case and different soil moisture states: (a) DA_100, (b) DA_70, and (c) DA_40. Latent and sensible heat fluxes are taken as positive away from the surface.

3. Influence on convection and precipitation in the basic configuration

a. *Surface energy balance*

Changes in soil moisture directly affect the partitioning of the incoming solar radiation into latent and sensible surface heat fluxes, as expected. Figure 2 highlights the decrease of surface latent heat fluxes from a maximum of about $0.8\,\mathrm{mm\,h^{-1}}$ in the wettest soil case (DA_100) to a nearly constant null value in the case with the driest soil (DA_40). Conversely, the surface sensible heat flux is inversely related to soil moisture, and its diurnal maximum increases from an initial value of

about 0.2 mm h^{-1} (DA_100) to a final value of almost 0.6 mm h^{-1} (DA_40). As a consequence, most of the incoming solar radiation in the DA_40 case is used to heat up the surface, which reaches a maximum temperature of 52°C, and to heat up the air above the surface, which reaches a maximum temperature of 37°C. Instead, in DA_100 the surface reaches a maximum temperature of about 37°C and the lowermost atmospheric layer heats up to 31°C in the early afternoon. Comparison of Figs. 2a and 2b also clearly highlights the effect of soil moisture that begins to limit the evaporation when starting from drier initial soil moisture conditions. Up to 1100 LST, DA_100 and DA_70 exhibit similar fluxes, but afterward the latent heat flux levels out in DA_70 and slightly decreases until the end of the day. The different temporal evolutions of net surface radiation visible in Fig. 2 during the afternoon hours reflect the different evolution of convection among the cases. In particular, the reduction of net surface radiation is due to cloud shading that changes accordingly to the different evolution of convective clouds.

Bowen ratio values averaged between 1200 and 1500 LST vary from 0.23 in the saturated case to 0.63 in the DA_70 case, 3.08 in the DA_60 case, and 118.36 in the driest case. We thus observe that the employed bare soil evaporation scheme produces near-null values when soil moisture approaches the wilting point. The almost complete shutdown of the latent heat flux in the DA_40 case may appear exaggerated but is observed over a semiarid region (e.g., Couvreux et al. 2012), which should be comparable to our bare soil setup. The reason for this behavior is that the bare soil evaporation scheme adopted in TERRA-ML, which is still used at the time of writing in the operational version of ICON, was adapted from the former generation of two layers soil models. As stated by Schulz et al. (2016), this scheme systematically overestimates (underestimates) evaporation under wet (dry) conditions, giving a wider variation of surface fluxes compared to observed ones. This is not of concern for this study as the important quantity determining the precipitation response is the latent heat flux, not the soil moisture, as will be shown in section 3c. Moreover, a larger variation in surface fluxes allows for a larger and hence more robust precipitation response.

b. *Convection and precipitation*

Figure 3 shows the evolution of the diurnal cycle of convection in both WA and DA cases, for two different values of the soil moisture as an example. All the simulations show a reasonable evolution of convection over time: clouds first appear in the late morning/early afternoon and dissipate in the late afternoon or even during the evening. After the growth of the first clouds in the late morning, rain is produced in less than 1 h, followed by a further vertical extension of the cloud tops that reach their maximum extent a few hours later: at this time ice is produced at the top and lasts until the late evening. The mean cloud thickness reaches lower values over drier soils, as found in Schlemmer et al. (2012), because of the higher LCL due to the decreased latent heat flux, while the cloud top remains unchanged. It can also be noticed that strong precipitation, as in the case of DA_100, leads to a collapse of the PBL around 1500 LST. The simulated small magnitude of the precipitation rate (insets in Fig. 3) reflects the limited spatial extension of the precipitating area, which covers at best 10%–15% of the domain. The values are on the order of magnitude of other LES studies that have investigated processes leading to the development of convection over midlatitude regions (e.g., Schlemmer et al. 2012).

More importantly, Fig. 3 reveals variations of convective precipitation as a function of soil moisture. Both the precipitation rates and the timing of convection respond to the changing soil moisture and hence surface fluxes. To better organize the results obtained for the cases presented in Table 2, domain-averaged accumulated precipitation and time of convection triggering are computed and shown in Fig. 4. The triggering of convection (LST) is defined by the first time instant when domain-averaged cloud cover exceeds 0.1. Convection is triggered 2 h earlier over the driest soil in the DA case, whereas being lagged in the WA case (Fig. 4a). The earlier triggering over dry soils in DA in contrast to WA can also be recognized in the precipitation rate time series of Fig. 3. These findings are in agreement with the results obtained by Findell and Eltahir (2003a) with their 1D model. The earlier triggering over dry soils in DA is due to the fact that the growth of the boundary layer through induced surface sensible heat fluxes is more efficient than moistening to trigger convection. In the WA case, in contrast, the lowering of LFC, due to surface moistening through latent heat fluxes, is the energetically most efficient mechanism, giving an earlier triggering over wet soils. However, in terms of precipitation, both cases show a decrease over dry soils. From Fig. 4b it can also be noted that above a degree of saturation of 80% and below a degree of saturation of 50%, the accumulated precipitation does not exhibit any dependency on soil moisture, most likely because of similar latent heat flux and triggering. This hypothesis will be explored in section 3c.

It should be noted that the relatively small amounts of precipitation do not allow the soil to recover from the losses caused by evaporation. In the DA_100 case, at the end of the simulated diurnal cycle, the uppermost layer

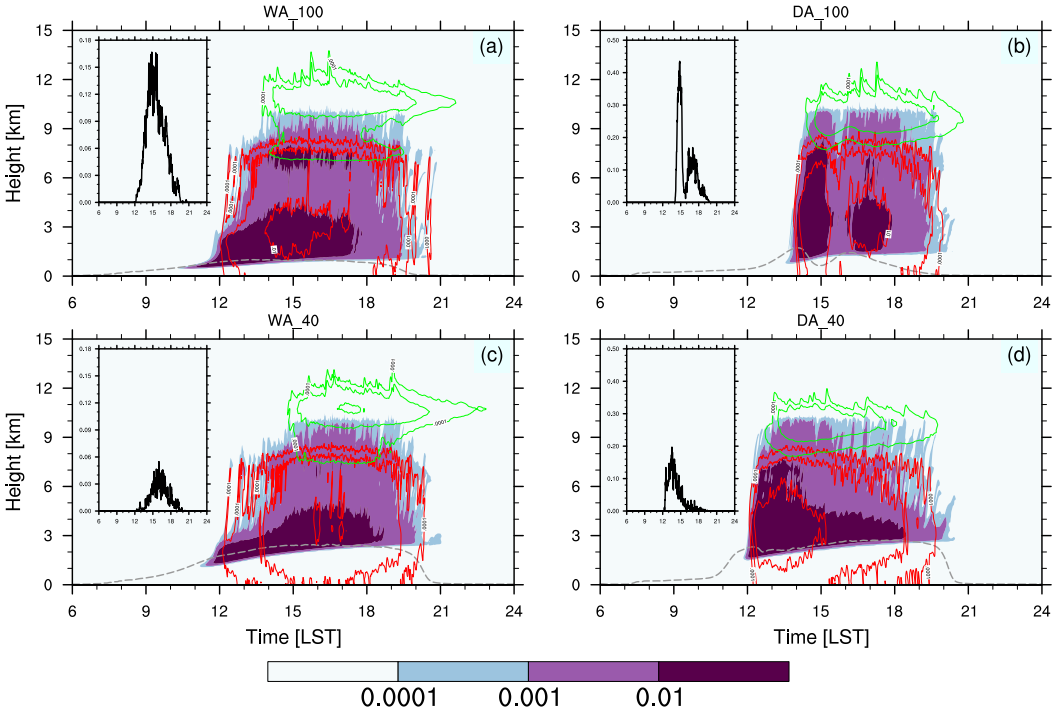

FIG. 3. Profile of domain-averaged quantities as functions of time for the (a),(c) WA and (b),(d) DA cases and two soil moisture states. Color shading represents the cloud water mixing ratio ($g\,kg^{-1}$), while cloud ice and rain mixing ratios are plotted by the green and red contour, respectively (same units and contour levels as cloud water). Note the logarithmic scale. The height of the boundary layer is shown by the gray dashed line (km). It is computed using the bulk Richardson number approach (see Seibert et al. 2000, and references therein). The *y* axis represents the height from the surface (km), while the *x* axis indicates the time of the simulation (LST). In the inset, surface precipitation rate ($mm\,h^{-1}$) is plotted as a function of time (LST).

of soil moisture reaches about 65% of its initial value, while in the DA_70 case it reaches almost 90%. This results from the fact that in DA_100 the saturated soil instantaneously produces runoff that brings the soil moisture to the field capacity, a model constraint, while in the other case soil moisture is lost only because of evaporation. Interestingly enough, in the DA_40 case the absence of evaporation allows a slight increase of soil moisture of about 1% of its initial value due to the recorded precipitation. Thus, in our simulations, wetter soils generally become drier while drier soils maintain their moisture reservoir, and the change in soil moisture over one day does not reflect the precipitation changes across the simulations. To avoid confusion between the soil moisture and the precipitation response, we will not refer to a negative soil moisture–precipitation coupling in the following but rather to a dry soil advantage when more precipitation is observed to fall over initially drier soils.

We further analyze the properties of the convective diurnal cycle through the computation of convective available potential energy (CAPE) and of cloud water and rain distribution. Figure 5 shows the time series of domain-averaged CAPE for both the WA and DA cases. It can be inferred that, regardless of the initial sounding, the energy available to feed convection decreases with soil moisture. This large, more than $1000\,J\,kg^{-1}$ difference at 1300 LST between 100% and 40% saturation is linked to different profiles of temperature and relative humidity in the first 1.5 km of the atmosphere due to the different Bowen ratios of the two simulations. In particular, both warming and drying of the PBL, as found over dry soils, lead to lower CAPE. This is consistent with the obtained decrease of precipitation rate (insets of Fig. 3) over drier soils, regardless of the initial sounding used. However, none of the simulations fully deplete their CAPE reservoir, which makes this simple explanation questionable. The decrease of CAPE over drier soils is consistent with what was already found by Barthlott and Kalthoff (2011) in more realistic simulations over southwestern Germany.

Figure 5 further reveals that in the DA case CAPE exhibits a very strong peak in the early afternoon and is rapidly depleted. Over soils with a soil moisture above 60% of the saturation value, however, large latent heat fluxes provide enough energy to rebuild a second peak

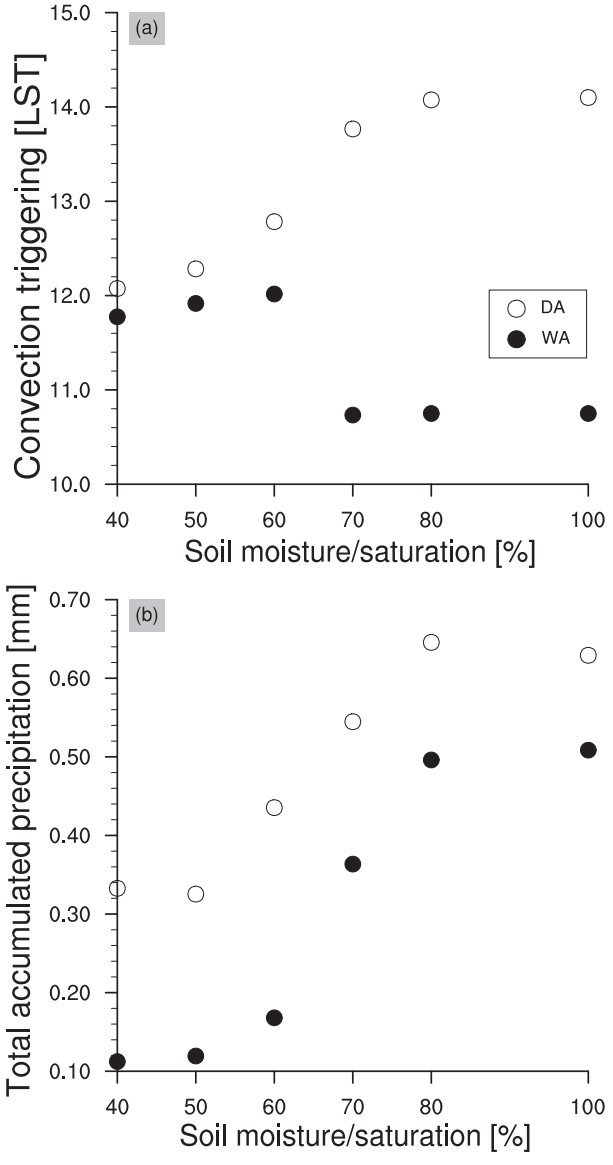

FIG. 4. (a) Time of convection triggering (LST), computed as the simulation time step when domain-averaged cloud cover exceeds a user-defined threshold of 0.1 and (b) total domain-averaged accumulated precipitation as a function of soil moisture scaled by the saturation value (%) for the DA and WA cases.

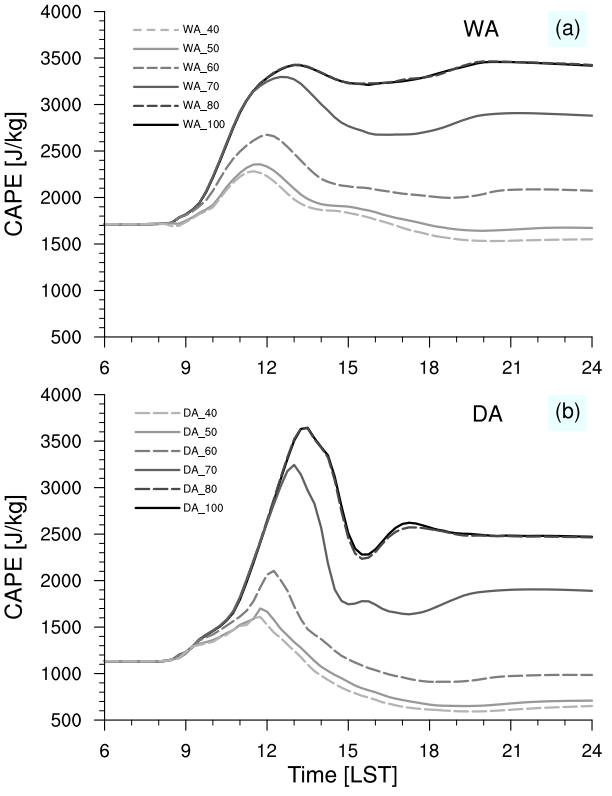

FIG. 5. Time series (LST) of domain-averaged CAPE (J kg^{-1}) for the (a) WA and (b) DA cases and different soil moisture states.

of CAPE in the late afternoon. This allows for a second development of convection. The presence of two convective events over wet soils that merge to one over dry soils is also clearly visible in Figs. 3b and 3d.

As an alternative to CAPE, Fig. 6 shows the full time and spatial average (indicated by angle brackets) of cloud water mixing ratio $\langle q_c \rangle$ and rain mixing ratio $\langle q_r \rangle$ as functions of soil moisture. Note that snow and cloud ice are not considered, given that they appear to be only minor components. The behavior of $\langle q_r \rangle$ is consistent with the behavior of the precipitation rate and shows a decrease toward drier soils irrespective of the initial atmospheric state. In contrast, the response of $\langle q_c \rangle$ depends on the initial sounding and does show an unexpected increase over dry soils in the DA case.

An increase in $\langle q_c \rangle$ may be caused either by a larger value of produced q_c or by the presence of longer-lived clouds. Larger values of produced q_c over drier soils seem unlikely, given the presence of a drier and warmer PBL regardless of the initial sounding. Longer-lived clouds may be created because of less evaporation of q_c or less conversion of q_c into q_r. Less evaporation of q_c over dry soils again seems unlikely, given the presence of a drier PBL. Hence, the only mechanism responsible for an increase of $\langle q_c \rangle$ over dry soils in the DA case must be linked to the efficiency in converting q_c into q_r. This appears as a reasonable hypothesis given what follows. The diurnal evolution simulated in the DA case over wet soil consists of two distinct convective events that progressively merge to one event over drier soils. The first event among the two shows larger precipitation rates and thicker clouds (see Fig. 3b). The lagged triggering of convection over wet soils in DA, due to reduced sensible heat flux, causes an accumulation of energy that is released abruptly when clouds are formed (Fig. 5) and

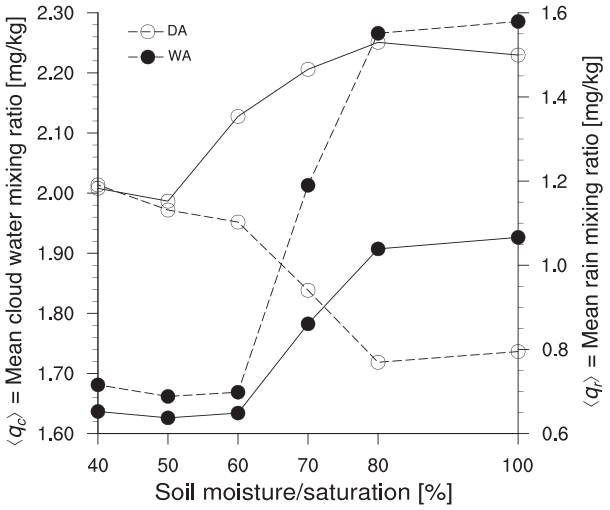

FIG. 6. Space-averaged, time-averaged cloud water mixing ratio (dashed lines) and rain mixing ratio (solid lines) for the DA (open circles) and WA (filled circles) case as a function of the degree of soil moisture saturation.

leads to a fast production of q_c. These local positive anomalies of cloud water are quickly converted into q_r, thus depleting the reservoir. This is mainly related to the fact that autoconversion processes and collection mechanisms in the microphysics depend nonlinearly on the amount of q_c [see Eqs. 5.107–5.112 in section 5.6 of Doms et al. (2011)]. Over dry soils the convection is less explosive so that the critical threshold is unlikely to be reached, and thus q_c is only partially depleted. When examining the values attained by q_c in DA_40, it appears that this variable has a larger mean but a lower spatial absolute maximum. On the other hand, DA_100 contains the highest value of q_c, although having a lower mean. In this regard, the WA case is equivalent to DA over dry soils: the slow growth of clouds does not produce high peaks of cloud water mixing ratio for any of the initial soil moisture, and q_c follows the moisture input from the surface.

c. *Under which conditions may drier soils receive more precipitation?*

The results outlined in the previous section seem to suggest that, in terms of total accumulated precipitation, there is no dry soil advantage. If the soil moisture is reduced, the surface latent heat flux decreases and thus the moisture flux from the surface to the atmosphere is limited. The atmosphere is not able to compensate for this lack of moisture contribution by becoming more efficient at converting water vapor into precipitation, the prerequisite to obtain more precipitation over drier soils. However, the previous section also showed that convection can indeed be triggered earlier over dry soils, which, under certain circumstances, may be able to overcompensate for the lack of moisture input.

To explore the feasibility of this scenario, the surface rain accumulated in time and spatially averaged R needs to be estimated a priori. Note that the terms rain and precipitation are used interchangeably as surface precipitation is always in liquid form. Moreover, the specification "domain averaged" is dropped given that every quantity is always averaged over the full domain area. Variable R (mm) is computed as

$$R = \sum_{i=1}^{N} \mathrm{RR}_i \times \Delta t = \sum_{i=1}^{N_1} \mathrm{RR}_i \times \Delta t + \sum_{i=1}^{N_0} 0 \times \Delta t = \sum_{i=1}^{N_1} \mathrm{RR}_i \times \Delta t, \quad (2)$$

that is, by summing the product of the instantaneous rain rate RR_i predicted by the model at the time step i ($\mathrm{mm\,h^{-1}}$) and the output time step Δt (h) over the entire simulation. The output time step is chosen small enough (30 s with a model time step of 2 s) to consider RR_i an instantaneous value. The total number of time steps N can be split into the number of rainy ($\mathrm{RR}_i > 0\,\mathrm{mm\,h^{-1}}$) events N_1 and the number of time steps with no rain N_0. By introducing a mean over rainy events $\widetilde{\mathrm{RR}} \equiv (1/N_1)\sum_{i=1}^{N_1} \mathrm{RR}_i$ Eq. (2) can be rewritten as

$$R = \sum_{i=1}^{N_1} \mathrm{RR}_i \times \Delta t = \widetilde{\mathrm{RR}} \times N_1 \times \Delta t \simeq \widetilde{\mathrm{RR}}(t_1 - t_0), \quad (3)$$

where now t_0 and t_1 indicate the time (LST) when precipitation begins and ends, respectively. It should be noted that the only used approximation, that is, $N_1 \times \Delta t \simeq (t_1 - t_0)$, holds for a typical precipitation intensity–time distribution over one diurnal cycle with no long temporal gap between precipitation events, which is indeed the case in the examples displayed in Fig. 3.

Finally, by assuming that $(t_1 - t_0)$ is approximately equal to the period when deep convective clouds are present on the domain, one can infer that R is related to three main parameters: the time when convection is triggered, which strongly depends on the atmospheric profile and exhibits either a wet or dry soil advantage in agreement with Findell and Eltahir (2003a); the time when convection dissipates; and finally, the mean rainfall rate.

In Fig. 7a the duration of precipitation $(t_1 - t_0)$ is computed for all the WA and DA simulations directly using the value of N_1 from the simulation output. The duration shows an interesting V-shaped distribution in the DA case, with a central minimum by a soil saturation of 70%, whereas such a central minimum is absent in the WA case. While convection is triggered earlier over

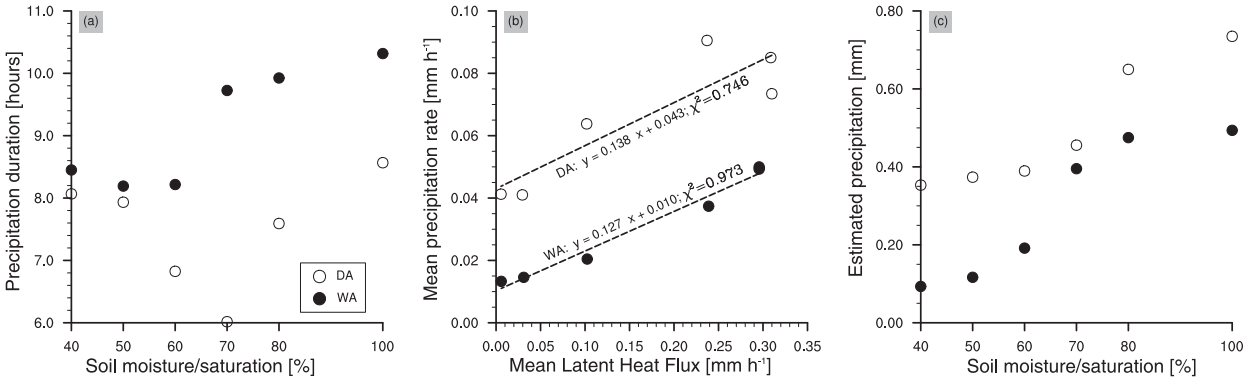

FIG. 7. (a) Precipitation duration as a function of the degree of soil moisture saturation. (b) Scatterplot of $\widetilde{RR}$ vs $\widetilde{LH}$: the equations represent the regression lines (slope and offset) together with the χ^2. (c) Accumulated precipitation R estimated by exploiting the linear fit and the duration term (see text for details).

drier soils than over wetter ones in DA, clouds dissipate later on wetter soils (see Fig. 3). This gives a total response with a central minimum. Concerning the variation of $\widetilde{RR}$ with soil moisture, it can be claimed that, based on the results of the previous section, $\widetilde{RR}$ scales with $\widetilde{LH}$, that is, the latent heat flux averaged over the precipitation duration. This is confirmed by Fig. 7b, which shows the values of $\widetilde{RR}$ and $\widetilde{LH}$ computed using data from both WA and DA simulations. The two cases even exhibit a similar slope, but different offsets. The slope of this line may be interpreted as a precipitation efficiency that, given the absence of large-scale moisture advection, is equivalent to the recycling ratio. It again suggests that, at least to a first order, the two soundings are not associated with fundamentally different convective dynamics once convection is triggered. There is nevertheless a larger scatter among the points in the DA case than in the WA case as also revealed by smaller Pearson chi-squared χ^2 values.

As a sanity check, Fig. 7c uses the linear fit of Fig. 7b to estimate $\widetilde{RR}$ and, combined with the diagnosed value of $t_1 - t_0$, to compute R. The resulting accumulated precipitation should be compared to the one diagnosed from the simulations in Fig. 4b. The relative errors of the different simulations range from about 2% to 20% for the WA case and from 1% to 15% for the DA case. The relative error averaged over all the simulations is about 10%. Although not perfect, the values predicted by this simple approximation resemble the simulated ones, and in particular the decrease of precipitation over dry soils is captured fairly well. We stress that our aim is not to predict the accumulated precipitation with the smallest possible error but rather to reproduce the overall observed behavior.

The advantage of Eq. (3) and of its parameterization is indeed that it splits the contribution of the total accumulated precipitation into two distinct terms, one favoring a wet soil advantage and one favoring either a dry or a wet soil advantage. Thus, it is possible to infer which precipitation duration would be needed to offset the decrease in $\widetilde{RR}$ due to changes in latent heat flux. For instance, Fig. 7b predicts that a decrease in latent heat flux from approximately 0.3 mm h^{-1} over wet soils to almost 0 mm h^{-1} over dry soils is accompanied by a half of the rain rate. This means that, in order to have more rain over dry soils, the duration term in Eq. (2) needs to balance a factor of at least 2. In other words, more than 16 h of continuous precipitation are needed to offset the lack of surface latent heat fluxes. This is unlikely to occur over one diurnal cycle.

These considerations are generalized in Fig. 8. There, the values of the slope and of the offset obtained in the

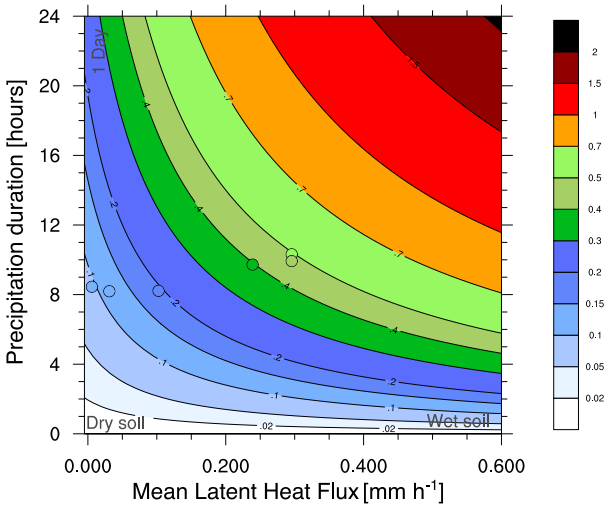

FIG. 8. Contour plot showing the estimated accumulated precipitation R (mm; shading) as a function of $\widetilde{LH}$ (mm h^{-1}) and $t_1 - t_0$ (h) for the WA case. Variable $\widetilde{RR}$ is computed by using the values of the slope and offset obtained in Fig. 7b for the WA case (see the text for more details). Dots are placed on the plot using the values of $\widetilde{LH}$, $t_1 - t_0$, and R directly diagnosed from the WA experiment.

linear regressions in Fig. 7b for the WA case are used to compute an estimated value of $\widetilde{RR}$, which is then used to obtain R. To do so we consider a wide variation of surface latent heat flux values (the x axis of Fig. 8) and precipitation durations less than 24 h (the y axis of Fig. 8). The result is a discrete function $R(\widetilde{LH}, t_1 - t_0)$, which is shown by the color-filled contour lines. The results of the WA case are represented by dots using the values of $(\widetilde{LH}, t_1 - t_0, R)$ obtained in every simulation. They reveal a good agreement with the theoretical estimates.

To compensate for a change in latent heat flux, one has to move along the isoline of accumulated precipitation in Fig. 8. Given the curvature of the isolines, only small changes in latent heat flux may be accommodated by changes in the duration, making the occurrence of more precipitation over drier soils unlikely. Moreover, the potential earlier triggering of convection over dry soils under certain atmospheric conditions, as in the DA case, is usually compensated by an equal shift of t_1, annihilating the triggering advantage. Hence, it may be concluded that the only possibility to obtain more precipitation over drier soils consists in not triggering convection over wet soils, which, for the tested situations, never happened.

Although this scenario is unlikely to occur, according to the values used to construct Fig. 8, some environmental conditions could lead to a weakening of the coupling. In fact, the curvature of the isolines in Fig. 8 depends on the slope and on the offset derived from the $\widetilde{RR}$–$\widetilde{LH}$ relationship. This is evident if rewriting Eq. (3) as

$$R = m\widetilde{LH}(t_1 - t_0) + q(t_1 - t_0), \tag{4}$$

where m and q are the slope and offset of the linear fit associated with the $\widetilde{RR}$–$\widetilde{LH}$ relationship, respectively. While the slope may be interpreted as the atmospheric efficiency in converting water vapor to rain, the offset may be interpreted as the overall availability of precipitable water, which depends both on the atmospheric state and on external forcing. Given that changes in m are weighted by the values of $\widetilde{LH} \ll 1$, one can imagine that changes of the same magnitude in q are more likely to affect R. Increasing m while keeping q constant causes a steepening of the contour lines for small values of $\widetilde{LH}$, making it even more unlikely to get more rain over drier soils. On the other hand, if q becomes large enough, the isolines become flatter even for small values of $\widetilde{LH}$ and the sensitivity of precipitation to latent heat flux is dampened. To get more rain over drier soil, q should be large enough so that the m term becomes negligible, and $t_1 - t_0$ should be zero only over wet soils. Another possibility would be to have a negative value of m. Since this does not seem to happen in the simulations presented up to now, we further investigate how environmental conditions and external forcing could concur to a dry soil advantage in the next section.

4. Sensitivity experiments

a. Additional cases

An inspection of the temporal evolution of cloud water and precipitation (not shown), similar to the one presented in Fig. 3, reveals a noticeable resemblance between the WA–WA2 and DA–DA2 cases, respectively. In particular, the simulations initialized with the DA2 atmospheric profile exhibit again two distinctive convective events over wet soils, merging into one single long-lived convective event over dry soils below a soil moisture saturation of 60%. The computation of $\langle q_c \rangle$ and $\langle q_r \rangle$ for the DA2 case also confirms the presence of an increase of $\langle q_c \rangle$ and of a decrease of $\langle q_r \rangle$ over dry soils, as observed in DA. In DA2 convection is triggered earlier over dry soils, as in DA, whereas in WA2 convective clouds appear first over wet soils, as in WA. As a consequence, the duration of precipitation for the DA2 case shows again a central minimum, whereas in WA2 a monotonic decrease is observed (not shown). The total accumulated precipitation nevertheless again decreases over dry soils irrespective of the initial sounding, and the $\widetilde{RR}$–$\widetilde{LH}$ linear relationship exhibits a comparable slope as in the DA and WA cases (Fig. 9). Because of the large spread observed in the DA2 case, the χ^2 value is smaller, while in the WA2 case it reflects the one obtained in WA. The only difference worth noting consists of the larger amount of accumulated precipitation observed in the DA2 case, which reflects the larger offset of the line in Fig. 9b, due to enhanced instability. The DA2 case is an example of a weaker coupling of soil moisture and precipitation due to a larger offset in the $\widetilde{LH}$–$\widetilde{RR}$ relationship (see the final part of section 3c). Nevertheless, the larger offset cannot reverse the relationship and lead to more precipitation over drier soils.

b. Transparent clouds

Making clouds transparent does not change the overall wet soil advantage (Fig. 10a), but the increase in the total accumulated precipitation with soil moisture is larger than in the DA case where CREs are included. This difference is linked to a larger sensitivity of the mean rain rate $\widetilde{RR}$ to the mean latent heat flux $\widetilde{LH}$ (see Fig. 10b). To explain this larger sensitivity, one can note that the surface energy balance is modified in DA_transp by the lack of CREs. The reduction of the net surface radiation seen in Fig. 2 between 1300

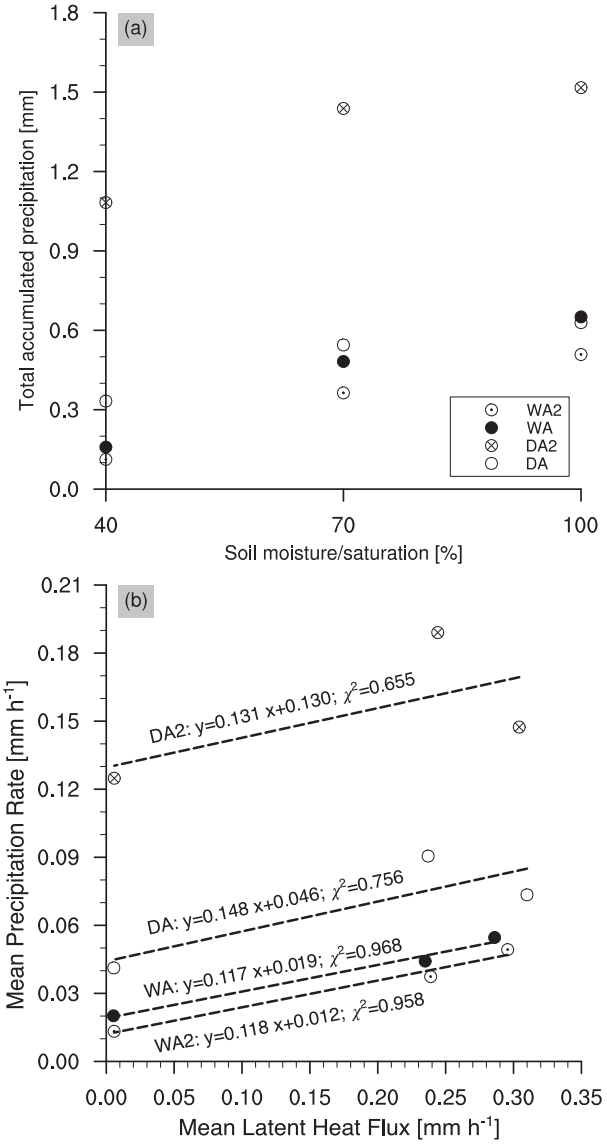

FIG. 9. (a) Total domain-averaged accumulated precipitation and (b) scatterplot of $\widetilde{RR}$ vs $\widetilde{LH}$ for simulations with different soil moisture and the DA, DA2, WA, and WA2 cases. The equations give the regression lines (slope and offset) together with the χ^2.

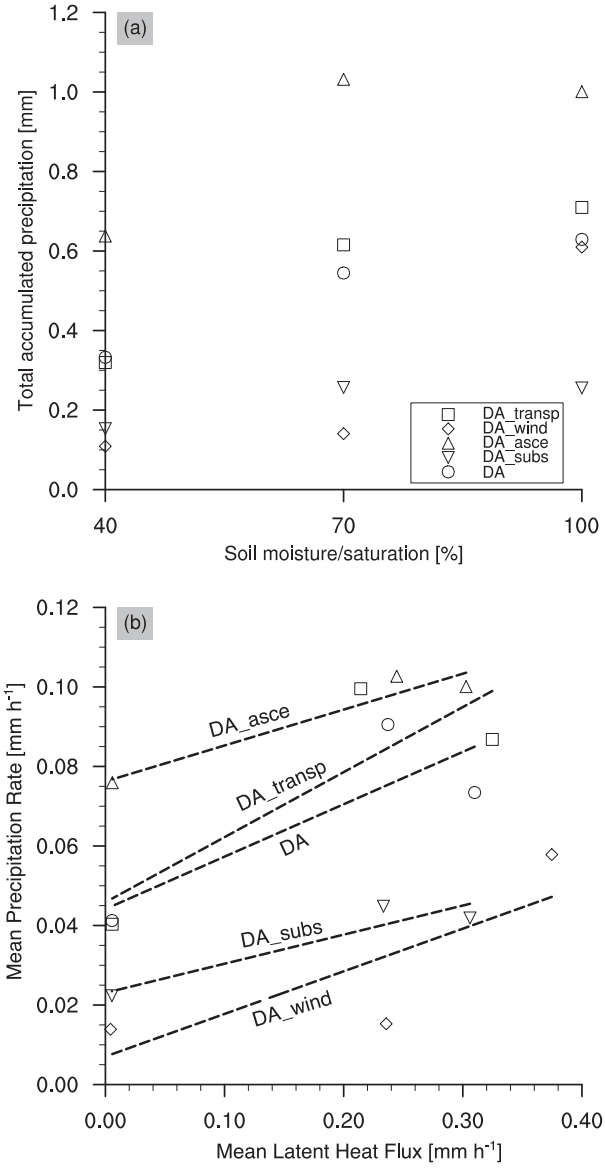

FIG. 10. As in Fig. 9, but for the experiments DA_subs, DA_asce, DA_wind, and DA_transp. The DA case is also included for the sake of comparison.

and 1600 LST in the DA_100 case, for instance, is absent when clouds are set transparent to radiation. The resulting increase of incoming shortwave radiation at the surface, on the order of 200 W m^{-2} in DA_transp compared to DA, is able to offset the opposing increase of surface outgoing longwave radiative flux of about 30 W m^{-2}. This surplus of radiative energy in DA_transp causes a slight increase of surface latent heat flux over wet soils because the simulation lies in an energy-limited regime because of the abundance of soil moisture, and a slight increase of surface sensible heat fluxes over dry soils, as the simulation belongs here to the soil moisture–limited regime. The magnitude of the soil moisture–precipitation coupling is enhanced. Hence, clouds act to dampen the soil moisture–precipitation coupling but cannot reverse its sign. These findings contrast with the results of Schär et al. (1999), where the presence of clouds further amplified the feedback due to the longwave CRE being stronger than the shortwave one. One reason for this discrepancy could be related to the fact that convective cloud features, including their interaction with radiation, are parameterized in the regional climate model (RCM) employed by Schär et al. (1999). Another reason could

be a distinct distribution of low and high clouds between the two studies.

c. Large-scale forcing

Figure 10a highlights a decrease of total accumulated precipitation over dry soils in DA_subs and DA_asce, thus confirming the presence of a wet soil advantage in both cases. However, with subsidence the convection is so heavily suppressed that the difference between the wettest soil and the driest soil in terms of precipitation is small. This is the result of two main factors. First, there is a smaller slope in the relationship between $\widetilde{RR}$ and $\widetilde{LH}$ (Fig. 10b), which is reasonable as convection is more strongly forced and less dependent upon the surface state. Second, the convection remains triggered earlier over dry soils as sensible heating is more efficient to break the inversion. Regarding DA_asce, even though the $\widetilde{RR}$–$\widetilde{LH}$ relationship exhibits a similar slope as in DA_subs, the duration term shows a different behavior, with a triggering time almost constant regardless of the soil moisture value. Introducing ascent forces the air to rise and to reach its LFC without having to rely too heavily on moistening or heating of the PBL through surface fluxes. The offset of the $\widetilde{RR}$–$\widetilde{LH}$ relationship is also modified in both the DA_subs and DA_asce cases compared to DA and reflects the additional source of buoyancy (more precipitation, larger offset when compared to DA) and the suppression of convection (less precipitation, smaller offset when compared to DA). These various differences are nevertheless not sufficient to alter the coupling sign. In both cases the points in Fig. 10b show no considerable spread, which is reflected in values of χ^2 higher than 0.9.

d. Winds

The inclusion of winds leads to a different evolution of the atmospheric state over time. Figure 11 shows a comparison of the vertically integrated cloud water and rain mixing ratios, and of the virtual potential temperature perturbation in the lowermost atmospheric level, for the DA and DA_wind simulations. The DA case does not show an appreciable degree of organization since only scattered convection is simulated, probably because of the absence of wind shear and of the homogeneous surface state (Chen and Avissar 1994). In contrast, the DA_wind simulation shows stronger and larger cold pools, as well as bigger clouds that tend to be organized along lines. Given that the strength of the cold pools is larger in DA_wind than in DA, one can argue that this case is indeed more organized, also considering the importance of cold pools on convective organization (Tompkins 2001). Although only qualitative, the differences between DA and DA_wind observed in Fig. 11 are reminiscent of the differences obtained in Schlemmer and Hohenegger (2014) between simulations with and without wind shear (see their Fig. 5).

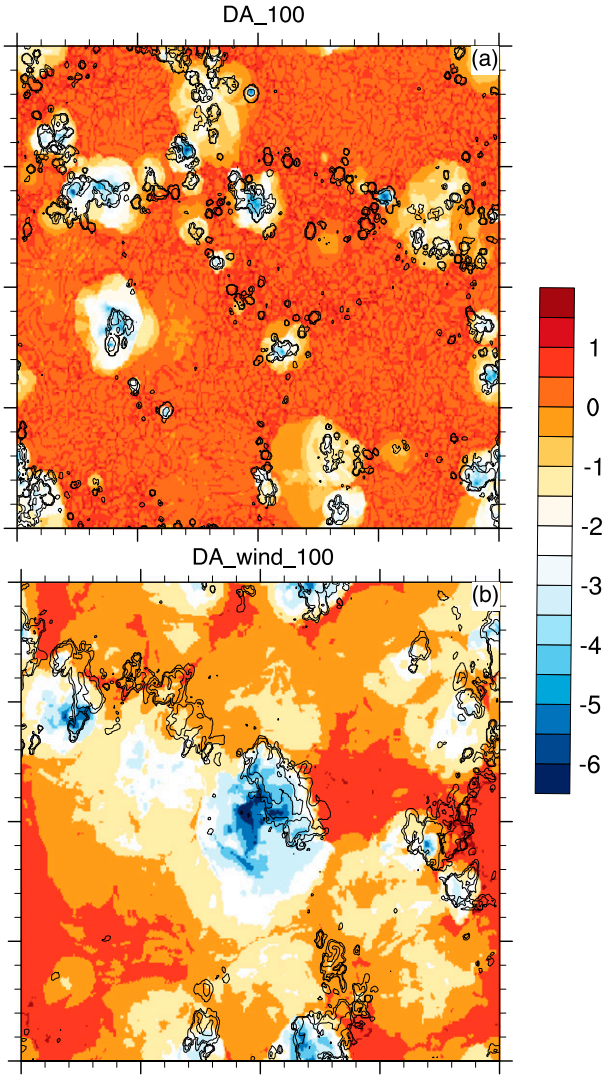

FIG. 11. Spatial distribution of clouds and cold pools in (a) DA_100 and (b) DA_wind_100. Color shading shows the near-surface (20 m) virtual potential temperature spatial anomaly (K), computed as deviation from the domain horizontal mean. Black contours show the vertically integrated sum of cloud water mixing ratio and rain mixing ratio: lines from 0.0001 to 0.01 every 0.005 (kg kg^{-1}). Both snapshots refer to 1730 LST.

Despite these differences in the spatial organization of convection, the coupling sign is not altered in this set of simulations. The DA_wind case still shows a decrease of total accumulated precipitation with soil moisture (see Fig. 10). The presence of larger winds increases the surface latent heat flux for a given value of soil moisture, as expected because of the drag-law formulation, but decreases the precipitation rate for a given latent heat flux. This decrease in precipitation rate may be related to CAPE, which is always smaller when compared to the DA

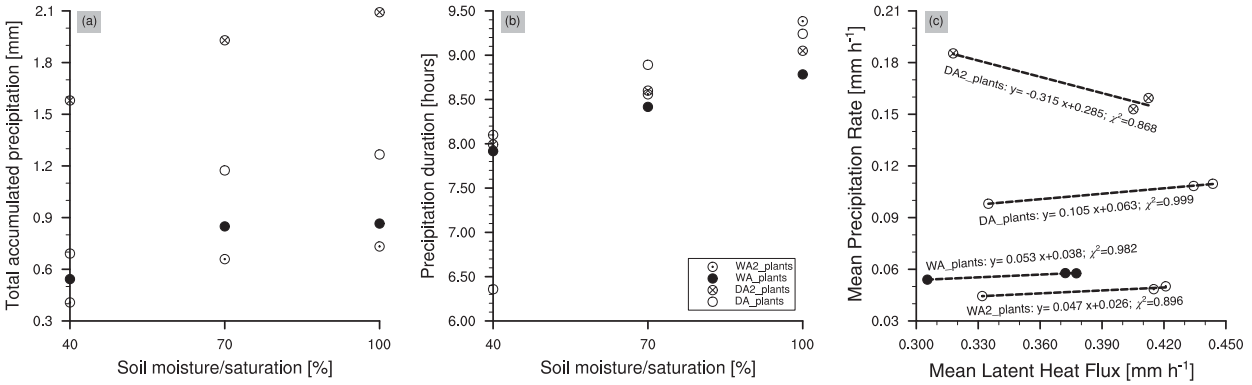

FIG. 12. (a) Total domain-averaged accumulated precipitation, (b) precipitation duration, and (c) scatterplot of $\widetilde{RR}$ vs $\widetilde{LH}$ for simulations WA_plants, DA_plants, WA2_plants, and DA2_plants. The equations represent the regression lines (slope and offset) together with the χ^2.

simulation. The presence of winds already at the beginning of the simulation induces more mixing and prevents an efficient buildup of instability, which would lead to an abrupt release of energy and ensuing higher precipitation rates (as already observed in section 3b). This results in a weaker dependency of $\widetilde{RR}$ on $\widetilde{LH}$ and, given similar changes in duration with soil moisture as in DA, leads to a weaker variation of total accumulated precipitation across the experiments. The weakening of the soil moisture–precipitation coupling in the presence of winds is consistent with Findell and Eltahir (2003b) and with the idea that stronger cold pools in DA_wind more strongly determine the precipitation rate evolution, making DA_wind less dependent on the surface state.

e. *Plants*

Whereas the water reservoir used by the evaporation from bare soil is limited to the uppermost soil layer, plants are able to extract moisture from deeper soil layers, thus contributing to larger values of surface latent heat flux over dry soils when compared to the bare soil evaporation case. An inspection of the surface fluxes time series confirms that, even in the DA_plants_40 case, latent heat flux reaches a maximum of 0.7 mm h^{-1}. Moreover, the presence of a deeper soil reservoir reduces the sensitivity of the latent heat flux to soil moisture, as can be recognized by comparing the variations in latent heat flux in Fig. 12c with the ones in Fig. 7b.

Given the larger value of latent heat flux, larger precipitation rates are recorded for a given soil moisture in the _plants simulations as compared to the control simulations (cf. Figs. 12a and 9a). More importantly, also in these experiments, total accumulated precipitation decreases over dry soils for all of the four considered atmospheric profiles. Splitting up the response in the contribution from duration and $\widetilde{RR}$ nevertheless shows a more subtle behavior. First, in WA_plants, WA2_plants, and DA_plants there is almost no sensitivity of $\widetilde{RR}$ to $\widetilde{LH}$, that is, the slopes of the regression lines are one-tenth of the ones observed in the bare soil cases. Second, the DA2_plants exhibits a negative slope. These differences to the bare soil case are partly an artifact in the sense that, due to their high latent heat flux, the cases with plants fall into the rightmost part ($\widetilde{LH} > 0.3$ mm h^{-1}) of Fig. 7a, where a strong scaling of $\widetilde{RR}$ with $\widetilde{LH}$ is also not observed in the bare soil case. The smaller spread of the points in Fig. 12c, which results in values of χ^2 close to 1, is probably due to this weaker dependency of $\widetilde{RR}$ to $\widetilde{LH}$.

5. Conclusions

In the present study, a state-of-the-art, high-resolution LEM is fully coupled to a land surface model to investigate the coupling between soil moisture and precipitation in an idealized setup. We use homogeneous initial soil moisture conditions and focus on the precipitation response to increase/decrease of the initial soil moisture. The soil moisture values considered are 40%, 50%, 60%, 70%, 80%, and 100% of the saturation value. To pursue this goal, the experimental framework proposed by Findell and Eltahir (2003a) is revisited by using the same atmospheric soundings as initial condition but allowing a full interaction of the atmosphere with the land surface over a complete diurnal cycle. These two soundings were recognized as representative of a wet soil advantage (more precipitation over wet soils) and of a dry soil advantage (more precipitation over dry soils), even though precipitation was not explicitly simulated in Findell and Eltahir (2003a). Furthermore, by using a grid resolution of 250 m, we aim at explicitly resolving moist convection.

The modeling framework is able to reproduce the expected sensitivity of the surface fluxes to soil moisture

and to simulate the typical convective evolution over one diurnal cycle. The triggering of convection happens earlier over dry soils than over wet soils for the dry soil advantage case and vice versa for the wet soil advantage case. This stands in agreement with the results of Findell and Eltahir (2003a) and confirms that certain atmospheric conditions may be preconditioned to different mechanisms of convection triggering. The cloud water content also shows a similar behavior with larger values over dry soil in the dry soil advantage case but larger values over wet soils in the wet soil advantage case. However, the precipitation is found to always decrease with decreasing soil moisture, irrespective of the initial sounding. This indicates the presence of a wet soil advantage. These different sensitivities of cloud water and precipitation to soil moisture can be explained by the way convective instability is exploited depending on the atmospheric state.

To understand these results and to infer under which conditions drier soils may receive more precipitation than wetter ones, we propose a simple model based on a linear fit to disentangle the effects of the surface on the precipitation amounts. The total domain-averaged accumulated precipitation is split into two main contributions: the value of precipitation rate averaged over the time when precipitation is occurring, and the duration of precipitation. While the latter depends upon the time of triggering and can exhibit a dry soil advantage, the precipitation rate is found to closely follow the values of the surface latent heat flux and thus always exhibits a wet soil advantage. The relationship between precipitation rate and surface latent heat flux is linear and, surprisingly enough, the slope of this linear relationship does not change appreciably with different atmospheric states. Using this simple linear relationship and combining it with a range of duration indicates that in our idealized setup a larger amount of precipitation is unlikely to be observed over drier soils. The relationship predicts that half of the latent heat flux, as obtained over soils with a 40% soil moisture saturation, must be offset by a doubling of precipitation duration. This is unlikely to occur over one diurnal cycle.

The effects of other factors on the coupling of soil moisture and precipitation, namely, cloud radiative effects, large-scale forcing, winds, and plants, are investigated by conducting further sensitivity experiments. All the experiments support a wet soil advantage. The strength of the coupling is reduced when large-scale effects or winds are included as the evolution of convection becomes more dictated by the large-scale forcing or the organization of convection by cold pools than by the surface state. The occurrence of clouds also leads to a weakening of the coupling due to their shortwave effects that overcompensate longwave changes and reduce the surface energy input. These results differ from other studies that employed models with parameterized convection, for example, Schär et al. (1999). Finally, plants also reduce the sensitivity of convection to the tested soil moisture through a much weaker dependency of latent heat flux on soil moisture.

Overall, our results suggest that changes in convection efficiency are unable to compensate for the reduction of evaporation over dry soils. These findings are only valid for those situations where changes in soil moisture do not affect or generate circulations. Moreover, a true feedback loop would imply that the increase in soil moisture due to precipitation affects the subsequent precipitation development. This is unlikely to occur over one diurnal cycle. One would expect a time scale of at least one week for the antecedent precipitation to directly influence the surface fluxes, as obtained by Duerinck et al. (2016).

Acknowledgments. This research was supported by the Hans Ertel Centre for Weather Research [Hans-Ertel-Zentrum für Wetterforschung (HErZ)], a collaborative project involving universities across Germany, and the DWD and was funded by the Federal Ministry of Transport and Digital Infrastructure [Bundesministerium für Verkehr und digitale Infrastruktur (BMVI)]. The simulations were performed using the facilities of the German Climate Computing Center [Detusches Klimarechenzentrum (DKRZ)] and in particular the new supercomputer Mistral. The comments of two anonymous reviewers are acknowledged, comments that allowed us to rephrase some parts of the manuscript, thus enhancing its overall clarity.

REFERENCES

Barthlott, C., and N. Kalthoff, 2011: A numerical sensitivity study on the impact of soil moisture on convection-related parameters and convective precipitation over complex terrain. *J. Atmos. Sci.*, **68**, 2971–2987, doi:10.1175/JAS-D-11-027.1.

Bryan, G. H., J. C. Wyngaard, and J. M. Fritsch, 2003: Resolution requirements for the simulation of deep moist convection. *Mon. Wea. Rev.*, **131**, 2394–2416, doi:10.1175/1520-0493(2003)131<2394:RRFTSO>2.0.CO;2.

Budyko, M., 1974: *Climate and Life.* International Geophysics Series, Vol. 18, Academic Press, 508 pp.

Chen, F., and R. Avissar, 1994: Impact of land-surface moisture variability on local shallow convective cumulus and precipitation in large-scale models. *J. Appl. Meteor.*, **33**, 1382–1401, doi:10.1175/1520-0450(1994)033<1382:IOLSMV>2.0.CO;2.

Clough, S., M. Shephard, E. Mlawer, J. Delamere, M. Iacono, K. Cady-Pereira, S. Boukabara, and P. Brown, 2005: Atmospheric radiative transfer modeling: A summary of the AER codes. *J. Quant. Spectrosc. Radiat. Transf.*, **91**, 233–244, doi:10.1016/j.jqsrt.2004.05.058.

Couvreux, F., C. Rio, F. Guichard, M. Lothon, G. Canut, D. Bouniol, and A. Gounou, 2012: Initiation of daytime local convection in a semi-arid region analysed with high-resolution simulations and AMMA observations. *Quart. J. Roy. Meteor. Soc.*, **138**, 56–71, doi:10.1002/qj.903.

Dickinson, R. E., 1984: Modeling evapotranspiration for three-dimensional global climate models. *Climate Processes and Climate Sensitivity*, *Geophys. Monogr.*, Vol. 29, Amer. Geophys. Union, 58–72.

Dipankar, A., B. Stevens, R. Heinze, C. Moseley, G. Zängl, M. Giorgetta, and S. Brdar, 2015: Large eddy simulation using the general circulation model ICON. *J. Adv. Model. Earth Syst.*, **7**, 963–986, doi:10.1002/2015MS000431.

Doms, G., and Coauthors, 2011: A description of the nonhydrostatic regional COSMO model: Part II: Physical parameterization. Consortium for Small-Scale Modeling Doc., 161 pp. [Available online at http://www.cosmo-model.org/content/model/documentation/core/cosmoPhysParamtr.pdf.]

Duerinck, H., R. van der Ent, N. van de Giesen, G. Schoups, V. Babovic, and P. J.-F. Yeh, 2016: Observed soil moisture–precipitation feedback in Illinois: A systematic analysis over different scales. *J. Hydrometeor.*, **17**, 1645–1660, doi:10.1175/JHM-D-15-0032.1.

Fermepin, S., and S. Bony, 2014: Influence of low-cloud radiative effects on tropical circulation and precipitation. *J. Adv. Model. Earth Syst.*, **6**, 513–526, doi:10.1002/2013MS000288.

Findell, K. L., and E. A. Eltahir, 2003a: Atmospheric controls on soil moisture–boundary layer interactions. Part I: Framework development. *J. Hydrometeor.*, **4**, 552–569, doi:10.1175/1525-7541(2003)004<0552:ACOSML>2.0.CO;2.

——, and ——, 2003b: Atmospheric controls on soil moisture–boundary layer interactions: Three-dimensional wind effects. *J. Geophys. Res.*, **108**, 8385, doi:10.1029/2001JD001515.

Fischer, E. M., S. Seneviratne, P. Vidale, D. Lüthi, and C. Schär, 2007: Soil moisture–atmosphere interactions during the 2003 European summer heat wave. *J. Climate*, **20**, 5081–5099, doi:10.1175/JCLI4288.1.

Ford, T. W., A. D. Rapp, S. M. Quiring, and J. Blake, 2015: Soil moisture–precipitation coupling: Observations from the Oklahoma Mesonet and underlying physical mechanisms. *Hydrol. Earth Syst. Sci.*, **19**, 3617–3631, doi:10.5194/hess-19-3617-2015.

Gentine, P., A. A. Holtslag, F. D'Andrea, and M. Ek, 2013: Surface and atmospheric controls on the onset of moist convection over land. *J. Hydrometeor.*, **14**, 1443–1462, doi:10.1175/JHM-D-12-0137.1.

Heinze, R., C. Moseley, L. N. Böske, S. Muppa, V. Maurer, S. Raasch, and B. Stevens, 2017a: Evaluation of large-eddy simulations forced with mesoscale model output for a multi-week period during a measurement campaign. *Atmos. Chem. Phys.*, **17**, 7083–7109, doi:10.5194/acp-17-7083-2017.

——, and Coauthors, 2017b: Large-eddy simulations over Germany using ICON: A comprehensive evaluation. *Quart. J. Roy. Meteor. Soc.*, **143**, 69–100, doi:10.1002/qj.2947.

Hinze, J. O., 1975: *Turbulence*. McGraw-Hill, 790 pp.

Hohenegger, C., A. Walser, W. Langhans, and C. Schär, 2008: Cloud-resolving ensemble simulations of the August 2005 alpine flood. *Quart. J. Roy. Meteor. Soc.*, **134**, 889–904, doi:10.1002/qj.252.

——, P. Brockhaus, C. S. Bretherton, and C. Schär, 2009: The soil moisture–precipitation feedback in simulations with explicit and parameterized convection. *J. Climate*, **22**, 5003–5020, doi:10.1175/2009JCLI2604.1.

Klemp, J., J. Dudhia, and A. Hassiotis, 2008: An upper gravity-wave absorbing layer for NWP applications. *Mon. Wea. Rev.*, **136**, 3987–4004, doi:10.1175/2008MWR2596.1.

Lilly, D. K., 1962: On the numerical simulation of buoyant convection. *Tellus*, **14**, 148–172, doi:10.3402/tellusa.v14i2.9537.

Maronga, B., and Coauthors, 2015: The Parallelized Large-Eddy Simulation Model (PALM) version 4.0 for atmospheric and oceanic flows: Model formulation, recent developments, and future perspectives. *Geosci. Model Dev.*, **8**, 2515–2551, doi:10.5194/gmd-8-2515-2015.

Miralles, D. G., M. J. van den Berg, A. J. Teuling, and R. A. M. de Jeu, 2012: Soil moisture–temperature coupling: A multiscale observational analysis. *Geophys. Res. Lett.*, **39**, L21707, doi:10.1029/2012GL053703.

——, A. J. Teuling, C. C. van Heerwaarden, and J. V.-G. de Arellano, 2014: Mega-heatwave temperatures due to combined soil desiccation and atmospheric heat accumulation. *Nat. Geosci.*, **7**, 345–349, doi:10.1038/ngeo2141.

Petch, J., A. Brown, and M. Gray, 2002: The impact of horizontal resolution on the simulations of convective development over land. *Quart. J. Roy. Meteor. Soc.*, **128**, 2031–2044, doi:10.1256/003590002320603511.

Pielke, R. A., 2001: Influence of the spatial distribution of vegetation and soils on the prediction of cumulus convective rainfall. *Rev. Geophys.*, **39**, 151–177, doi:10.1029/1999RG000072.

Randall, D. A., and D. G. Cripe, 1999: Alternative methods for specification of observed forcing in single-column models and cloud system models. *J. Geophys. Res.*, **104**, 24 527–24 545, doi:10.1029/1999JD900765.

Richards, L. A., 1931: Capillary conduction of liquids through porous mediums. *J. Appl. Phys.*, **1**, 318–333, doi:10.1063/1.1745010.

Rotunno, R., J. B. Klemp, and M. L. Weisman, 1988: A theory for strong, long-lived squall lines. *J. Atmos. Sci.*, **45**, 463–485, doi:10.1175/1520-0469(1988)045<0463:ATFSLL>2.0.CO;2.

Schär, C., D. Lüthi, U. Beyerle, and E. Heise, 1999: The soil–precipitation feedback: A process study with a regional climate model. *J. Climate*, **12**, 722–741, doi:10.1175/1520-0442(1999)012<0722:TSPFAP>2.0.CO;2.

Schlemmer, L., and C. Hohenegger, 2014: The formation of wider and deeper clouds as a result of cold-pool dynamics. *J. Atmos. Sci.*, **71**, 2842–2858, doi:10.1175/JAS-D-13-0170.1.

——, ——, J. Schmidli, and C. Schär, 2012: Diurnal equilibrium convection and land surface–atmosphere interactions in an idealized cloud-resolving model. *Quart. J. Roy. Meteor. Soc.*, **138**, 1526–1539, doi:10.1002/qj.1892.

Schrodin, R., and E. Heise, 2002: A new multi-layer soil model. *COSMO Newsletter*, No. 2, Consortium for Small-Scale Modeling, Offenbach, Germany, 149–151. [Available online at http://www.cosmo-model.org/content/model/documentation/newsLetters/newsLetter02/newsLetter_02.pdf.]

Schulz, J.-P., G. Vogel, C. Becker, S. Kothe, U. Rummel, and B. Ahrens, 2016: Evaluation of the ground heat flux simulated by a multi-layer land surface scheme using high-quality observations at grass land and bare soil. *Meteor. Z.*, **25**, 607–620, doi:10.1127/metz/2016/0537.

Seibert, P., F. Beyrich, S.-E. Gryning, S. Joffre, A. Rasmussen, and P. Tercier, 2000: Review and intercomparison of operational methods for the determination of the mixing height. *Atmos. Environ.*, **34**, 1001–1027, doi:10.1016/S1352-2310(99)00349-0.

Sommeria, G., and J. Deardorff, 1977: Subgrid-scale condensation in models of nonprecipitating clouds. *J. Atmos. Sci.*, **34**, 344–355, doi:10.1175/1520-0469(1977)034<0344:SSCIMO>2.0.CO;2.

Stevens, B., S. Bony, and M. Webb, 2012: Clouds On-Off Klimate Intercomparison Experiment (COOKIE). EUCLIPSE Tech. Rep., 12 pp. [Available online at http://www.euclipse.eu/downloads/Cookie.pdf.]

Tawfik, A. B., P. A. Dirmeyer, and J. A. Santanello Jr., 2015: The heated condensation framework. Part I: Description and Southern Great Plains case study. *J. Hydrometeor.*, **16**, 1929–1945, doi:10.1175/JHM-D-14-0117.1.

Taylor, C. M., A. Gounou, F. Guichard, P. P. Harris, R. J. Ellis, F. Couvreux, and M. De Kauwe, 2011: Frequency of Sahelian storm initiation enhanced over mesoscale soil-moisture patterns. *Nat. Geosci.*, **4**, 430–433, doi:10.1038/ngeo1173.

——, R. A. de Jeu, F. Guichard, P. P. Harris, and W. A. Dorigo, 2012: Afternoon rain more likely over drier soils. *Nature*, **489**, 423–426, doi:10.1038/nature11377.

Tompkins, A. M., 2001: Organization of tropical convection in low vertical wind shears: The role of cold pools. *J. Atmos. Sci.*, **58**, 1650–1672, doi:10.1175/1520-0469(2001)058<1650:OOTCIL>2.0.CO;2.

Trenberth, K. E., 1999: Atmospheric moisture recycling: Role of advection and local evaporation. *J. Climate*, **12**, 1368–1381, doi:10.1175/1520-0442(1999)012<1368:AMRROA>2.0.CO;2.

Van der Ent, R. J., H. H. Savenije, B. Schaefli, and S. C. Steele-Dunne, 2010: Origin and fate of atmospheric moisture over continents. *Water Resour. Res.*, **46**, W09525, doi:10.1029/2010WR009127.

VanZanten, M. C., and Coauthors, 2011: Controls on precipitation and cloudiness in simulations of trade-wind cumulus as observed during RICO. *J. Adv. Model. Earth Syst.*, **3**, M06001, doi:10.1029/2011MS000056.

Wan, H., and Coauthors, 2013: The ICON-1.2 hydrostatic atmospheric dynamical core on triangular grids—Part 1: Formulation and performance of the baseline version. *Geosci. Model Dev.*, **6**, 735–763, doi:10.5194/gmd-6-735-2013.

Wang, G., Y. Kim, and D. Wang, 2007: Quantifying the strength of soil moisture–precipitation coupling and its sensitivity to changes in surface water budget. *J. Hydrometeor.*, **8**, 551–570, doi:10.1175/JHM573.1.

Zängl, G., D. Reinert, P. Rípodas, and M. Baldauf, 2015: The ICON (ICOsahedral Non-hydrostatic) modelling framework of DWD and MPI-M: Description of the non-hydrostatic dynamical core. *Quart. J. Roy. Meteor. Soc.*, **141**, 563–579, doi:10.1002/qj.2378.